MTLA 40 (2025) 102412

Contents lists available at ScienceDirect

Materialia

journal homepage: www.elsevier.com/locate/mtla

Enhanced deformability of TiC in Mo-Ti-C ternary system by off-stoichiometry

Shuntaro Ida [a,1,*], Eri Nakagawa [b], Viola Paul [b], Takahito Ohmura [b], Kyosuke Yoshimi [a]

[a] Department of Materials Science, Graduate School of Engineering, Tohoku University, 6-6-02 Aramaki Aza Aoba, Aoba-ku, Sendai, 980-8579, Japan
[b] Research Center for Structural Materials, National Institute for Materials Science, 1-2-1 Sengen Tsukuba Ibaraki, 305-0047 Japan

ARTICLE INFO

Keywords:
Deformation
TiC
Off-stoichiometry
Micropillar compression

ABSTRACT

The deformation behavior of B1-type stoichiometric TiC and off-stoichiometric $(Ti_{0.96}, Mo_{0.04})C_{0.67}$ was investigated by micropillar compression test utilizing an in situ scanning electron microscope. The yield stress of $(Ti_{0.96}, Mo_{0.04})C_{0.67}$ was found to be sufficiently lower than that of the stoichiometric TiC. In addition, the {001}<1$\bar{1}$0>, {110}<1$\bar{1}$0>, and {111}<1$\bar{1}$0> slip systems were identified to be active during the plastic deformation of $(Ti_{0.96}, Mo_{0.04})C_{0.67}$. The critical resolved shear stresses of these slip systems decreased in the following order: {110}<1$\bar{1}$0> (5.6 GPa), {001}<1$\bar{1}$0> (5.0 GPa), and {111}<1$\bar{1}$0> (4.4 GPa). In contrast to the stoichiometric TiC, which underwent complete fracture at a relatively early stage of deformation, $(Ti_{0.96}, Mo_{0.04})C_{0.67}$ deformed under >10 % plastic strain without fracturing, with crack preferentially initiating along the {001} plane. The findings demonstrate that the off-stoichiometry of $(Ti_{0.96}, Mo_{0.04})C_{0.67}$ improves plastic deformability and has a suppressive effect on crack propagation. The enhanced deformability may be attributed to the significantly reduced shear modulus caused by off-stoichiometry.

1. Introduction

B1-type MX compounds are composed of a transition metal at the M site and a nonmetallic element at the X site. Although the atomic arrangements of both sites are identical to those observed in the face-centered cubic (FCC) structure, the M and X sites are shifted in the [1/2 0 0] direction. Titanium carbide (TiC) is a hard material with a high melting point (3067°C) and a low density (4.93 g/cm^3), rendering it a promising strengthening phase for use in high-temperature materials [1–4]. Consequently, carbides are used as coatings for tool steels and as hardening phases in cermets [2,5–9]. However, TiC has a relatively low fracture toughness of ~3 MPa(m)$^{1/2}$ at room temperature [10,11]. In particular, when the B1-type TiC in phase equilibrium with the metallic phase is close to the stoichiometric composition, such as in the case of Fe-Ti-C ternary alloys, the ductility of the alloy decreases with an increasing TiC volume fraction [12]. These properties therefore limit the application range of B1-type MX compounds.

Previous studies have shown that the cleavage fracture plane of B1-type TiC is the {001} plane [13,14] owing to its low surface energy [15,16]. In terms of the deformation of B1-type MC carbides at room temperature, it has been described that group IV transition metal carbides exhibit high strength and hardness characteristics, but a low ductility, leading to the {110}[1$\bar{1}$0] slip system being the most active [17–19]. In contrast, the group V transition metal carbides are more ductile, with the {111}[1$\bar{1}$0] slip system being more active [17–22]. By combining group IV and V elements at the M site, it is possible to obtain {110}[1$\bar{1}$0] and {111}[1$\bar{1}$0] slip systems, thereby enhancing both the ductility and the strength [23].

For the B1-type TiC that is in equilibrium with the metallic phase, a sufficiently large degree of off-stoichiometry can exist. In the case of off-stoichiometric TiC, various metallic elements (M) substitute at the Ti site, whereas several nonmetallic elements (X), including nitrogen and oxygen, substitute at the C site. This leads to structural vacancies and the generation of a (Ti, M)X_x compounds. Such off-stoichiometry alters the physical properties of the material, and the defect structure, phase stability, and elastic modulus of (Ti, M)X_x have been investigated [24–30]. Additionally, changes in binding energy and band structure of off-stoichiometric TiX_x have been reported [31,32], and the properties

* Corresponding author.
E-mail addresses: shuntaro_ida@jfcc.or.jp (S. Ida), NAKAGAWA.Eri@nims.go.jp (E. Nakagawa), PAUL.Viola@nims.go.jp (V. Paul), OHMURA.Takahito@nims.go.jp (T. Ohmura), yoshimi@material.tohoku.ac.jp (K. Yoshimi).
[1] Present address: Materials Research and Development Laboratory, Japan Fine Ceramics Center, 2–4–1 Mutsuno, Atsuta-ku, Nagoya, 456–8587 Japan.

https://doi.org/10.1016/j.mtla.2025.102412
Received 10 April 2025; Accepted 15 April 2025
Available online 17 April 2025

and structures of multicomponent B1-type MX compounds with [33–35] and without [36–41] vacancies have been investigated using ab initio calculations and experiments. Furthermore, the phase equilibria between the metal solid solution phase and TiC and the elastic properties of (Ti, Mo)C_x in the Mo-Ti-C ternary system have also been examined [42,43]. Based on the classical Pugh and Pettifor criteria, which are commonly employed by metallurgists to predict whether a material is brittle or ductile, (Ti, Mo)C_x may exhibit enhanced ductility owing to off-stoichiometry [44,45].

TiC is generally prepared using methods such as hot pressing, hot isostatic pressing, self-combustion synthesis, and discharge plasma sintering. However, these processes inevitably lead to the formation of voids and compositional changes during sample preparation [46]. Consequently, accurate evaluation of the mechanical properties of bulk TiC remains challenging.

In this study, the deformation behavior of B1-type (Ti, Mo)C_x were investigated using micropillar compression test on alloys prepared via the arc melting technique, which minimizes void formation. Since the phase equilibria in the Mo-Ti-C ternary system are well established, the composition of (Ti, Mo)C_x can be precisely controlled by equilibrating the alloy [42].

2. Experimental

The compositions of the samples employed in the current study were Mo-46.8 %Ti-5.0 %C and Ti-50 %C. All compositions are expressed as atomic percentages unless otherwise noted. The raw materials were pure Mo (99.99 wt %), pure Ti (99.9 wt %), and pure TiC powder (99 wt %). The Mo-46.8Ti-5.0C alloy was melted using an arc-melting technique to produce an ingot of ~10 cm^3. Each ingot was melted five times and was turned over after each time to avoid segregation. To reach phase equilibria, heat treatment was carried out at 1800°C for 72 h in an Ar atmosphere. It has been previously reported that at a temperature of 1800°C, Mo-46.8Ti-5.0C is in equilibrium with a Mo solid solution and ($Mo_{0.04}$, $Ti_{0.96}$)$C_{0.67}$ [42]. In addition, the Ti-50C alloy was fabricated by spark plasma sintering (SPS) at 1650°C and 65 MPa for 10 min using pure TiC powders. The microstructure was observed by field-emission (FE) scanning electron microscopy (SEM). A focused ion beam (FIB) was employed to fabricate the micropillar compression test specimens, and electron backscatter diffraction (EBSD) was used to measure the orientation of the micropillar compression test specimens. The dimensions of the micropillar compression test specimens were 1 μm × 1 μm × 2 μm, and their compression orientations were <001>, <011>, and <111>. Deformation of the micropillar compression test piece was measured on a PI 89 system (Bruker Hysitron) attached to the SEM. A diamond flat-punch indenter was used for the compression tests with a strain rate of 2×10^{-4} s^{-1}. Alignment of the center axes of the indenter and the specimen was confirmed by ensuring that the curve returned to its original state after unloading and subsequent reloading during the deformation process. The stress–strain curve was plotted based on the load and displacement measured from the micropillar compression test and the dimensions of the test piece before testing. The yield stress was defined as 0.2 % proof stress, calculated from the slope of the linear portion of the stress–strain curve, which is defined as the elastic region.

3. Results and discussion

3.1. Microstructure

Fig. 1 shows isothermal cross-section of the Mo-Ti-C ternary system at 1800°C [42], together with the scanning electron images (SEIs) of the corresponding specimens. As shown in Fig. 1(b), Ti-50C is composed of stoichiometric equiaxed TiC grains with a grain size of ~10 μm. However, numerous voids measuring a few micrometers in size are also evident, which may have formed during sample preparation. These results suggest the possibility of fabricating micropillar compression specimen while avoiding void generation. In contrast, the Mo-46.8Ti-5.0C was composed of Mo solid solution and ($Mo_{0.04}$, $Ti_{0.96}$)$C_{0.67}$ with grain sizes of ~10 μm (Fig. 1(c)). No voids were observed in the ($Mo_{0.04}$, $Ti_{0.96}$)$C_{0.67}$ grains, which were sufficiently large to fabricate micropillar compression specimen.

3.2. Micropillar compression test

Fig. 2 illustrates the stress–strain curves derived from the micropillar compression tests conducted on the stoichiometric TiC. In all curves, the stress exhibited a gradual increase immediately after loading, followed by a linear increase owing to elastic deformation, and then a gradual increase owing to plastic deformation. The slow increase immediately after loading may be attributed to the fact that the indenter and specimen surfaces were not in complete contact. In the <001> compression direction, the stress was significantly lower than that observed in the

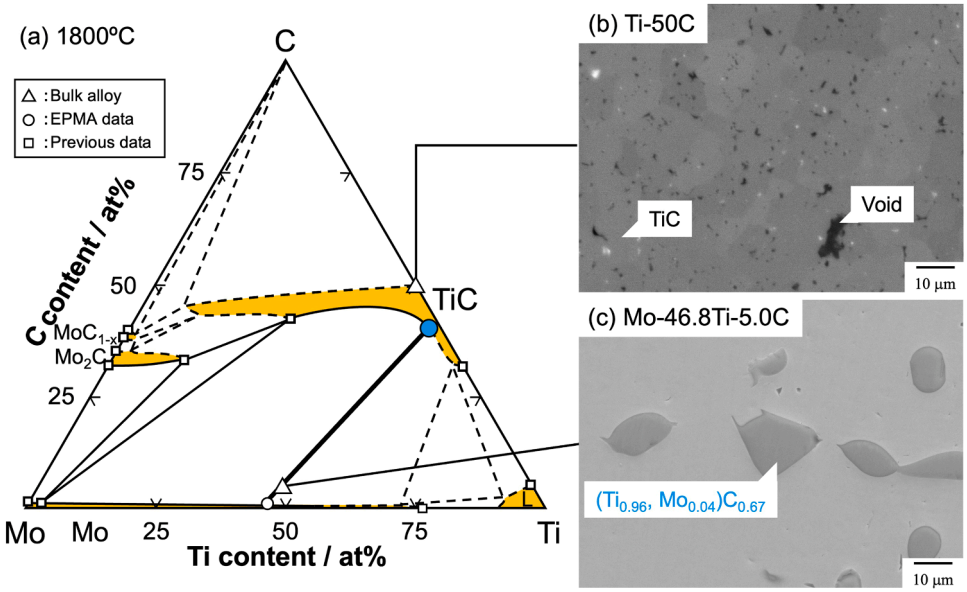

Fig. 1. (a) Isothermal section of the Mo-Ti-C ternary system at 1800 °C, and (b, c) SEIs of the samples [42].

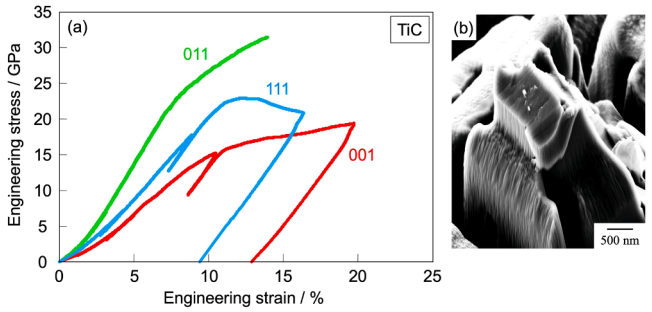

Fig. 2. Stress–strain curves of the stoichiometric TiC obtained from micropillar compression tests along the <001>, <011>, and <111> compression directions (a), and the fractured specimen after testing along the <011> compression direction (b).

<011> and <111> directions, implying that cracks may form even during the elastic deformation stage. In the <111> compression direction, the slope of the curve during plastic deformation exhibited a negative value immediately after plastic deformation. This can be attributed to the cracking that occurs during the early stages of plastic deformation. Conversely, no such phenomenon was observed for the <011> compression direction; instead, fracture occurred at a relatively early stage of plastic deformation (Fig. 2 (b)). Based on the results obtained for the <011> and <111> compression orientations, the yield stress of the stoichiometric TiC was determined to be ≥20 GPa.

Fig. 3 shows the stress–strain curve of $(Ti_{0.96}, Mo_{0.04})C_{0.67}$ obtained from the micropillar compression test (001) in the <001> compression direction. The SEI of the specimen recorded in situ is also shown, wherein the sides of the specimen were oriented along the (100) and (010) planes. As observed in the case of TiC, the stress exhibited a gradual increase immediately after loading, followed by a linear increase owing to elastic deformation, and then a gradual increase owing to plastic deformation. The slopes of the unloading process within the elastic deformation range, the loading process within the elastic deformation range, and the unloading process within the plastic deformation range differed slightly from one another. This may be attributed to incomplete contact between the indenter and the specimen surface, as well as a slight offset between the center axes of the indenter and the specimen. Prior to performing these measurements, the surface of the specimen was observed to be smooth (Fig. 3(b)), and the smoothness was retained during the elastic deformation phase (Fig. 3(c)). In contrast, the formation of slip lines was evident on the (100) plane after the onset of plastic deformation (Fig. 3(d)). Moreover, a comparison of the specimen sizes before and after the measurements (see Figs. 3(b) and 3(e)) indicated that plastic strain was introduced, and the degree of plastic strain was consistent with that observed in the stress–strain

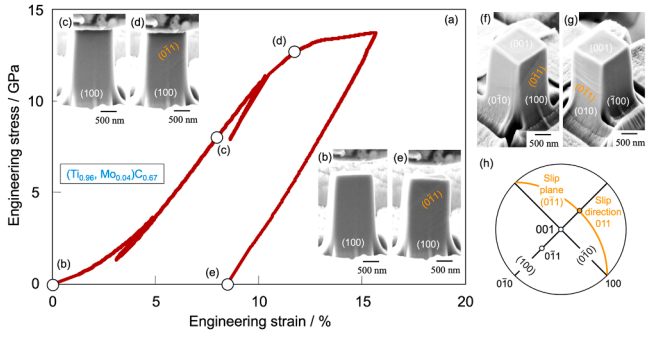

Fig. 3. (a) Stress–strain curve of $(Ti_{0.96}, Mo_{0.04})C_{0.67}$ (001-A) obtained from the micropillar compression test along the <001> compression direction, and (b–e) SEIs of the specimen during in situ observations. (f) SEIs of the specimen after the test, (h) Stereographic analysis of the slip lines.

curve. Notably, this result confirms the occurrence of plastic deformation in $(Ti_{0.96}, Mo_{0.04})C_{0.67}$.

As shown in Fig. 3(f), the slip line on the (010) plane of the specimen side fell along the [100] direction, and the angle between the slip line on the (100) plane and the [001] direction was ~45° Consequently, the slip line on the (100) plane was determined to fall along the [011] direction (Fig. 3(g)), indicating that dislocation was active in the $(0\bar{1}1)$ plane (Figs. 3(f) and 3(g)). Furthermore, the slip line on the (010) plane of the specimen side exhibited a step owing to deformation, suggesting that the dislocation glided in the [011] direction (Fig. 3(g)). This is consistent with previously reported results [17–23], as well as the fact that the [011] direction is the closest packing direction in the B1-type structure. These results indicate that the $\{110\}\langle 1\bar{1}0\rangle$ slip system was active during the plastic deformation of $(Ti_{0.96}, Mo_{0.04})C_{0.67}$ along the [001] compression direction.

Fig. 4 shows the stress–strain curves obtained from the micropillar compression tests using $(Ti_{0.96}, Mo_{0.04})C_{0.67}$ in the <001>, <011>, and <111> compression directions. The SEIs of the specimens after testing are also presented. In the 001–B and 001–C compression directions, equivalent Young's moduli, yield stresses, and the slope of the curve during plastic deformation were obtained even when the strain was increased compared to the 001–A compression direction, as illustrated in Fig. 3. Furthermore, in the <011> compression direction, similar Young's moduli, yield stresses were obtained in all three tests (Fig. 4(b)); the same trend was also observed in the <111> compression direction. However, 111-A and 111-C compressive directions exhibited negative slope of the curve during plastic deformation, which can be attributed to the formation of cracks during plastic deformation (Fig. 4(c)).

Subsequently, the elastic and plastic deformation behaviors of $(Ti_{0.96}, Mo_{0.04})C_{0.67}$ were investigated in all three compression directions. More specifically, in the <001> compression direction, dislocations were active on the $(0\bar{1}1)$ plane, even when the specimen sides constituted the (110) and $(\bar{1}10)$ planes (Figs. 4(d) and 4(e)). Although the slip direction could not be identified precisely in this case, it is likely correlated with the [011] direction since the slip plane included the [011] direction, and the entire specimen deformed in the [011] direction. Therefore, the slip system was determined to be $\{110\}\langle 1\bar{1}0\rangle$. In the <011> compression direction with specimen sides corresponding to the (100) and $(0\bar{1}1)$ planes, the slip line on the (100) side face was oriented in the $[0\bar{1}1]$ direction (Fig. 4(f) and (g)). The angle between the slip lines on the side of the specimen in the $(0\bar{1}1)$ and [011] directions was determined to be ~55°, indicating that the slip line is in the $[\bar{2}11]$ direction. These observations indicate that dislocations were active on the (111) plane. Considering that deformation steps were observed on all specimen sides and that both $[\bar{1}01]$ and $[\bar{1}10]$ were included in the slip plane, it can be inferred that the slip direction was $\langle 1\bar{1}0\rangle$. Therefore, the slip system along the [011] compression direction was determined to be $\{111\}\langle 1\bar{1}0\rangle$. When the diagonal lines of the basal plane were oriented in the $[1\bar{1}0]$ and $[\bar{1}\bar{1}2]$ directions in the <111> compression direction (Figs. 4(h) and 4(i)), the angles formed by the trace of the slip plane and the <111> direction were equal on both sides. Therefore, (100) was identified as the slip plane based on the angle between the slip and (111) planes. As the entire specimen appeared to deform in the <110> direction, which was included in the slip plane, the slip direction was inferred to be <110>. Therefore, the active slip system in the <111> compression direction was determined to be $\{001\}\langle 1\bar{1}0\rangle$.

Table 1 summarizes the results of the micropillar compression tests performed on the $(Ti_{0.96}, Mo_{0.04})C_{0.67}$ specimen, wherein the critical resolved shear stress (CRSS) was calculated using the experimentally obtained compression direction, slip system, and yield stress. In all compression orientations, the yield stress of $(Ti_{0.96}, Mo_{0.04})C_{0.67}$ was significantly lower than that of TiC (≥20 GPa), exhibiting a larger plastic strain without fracture. This indicates that $(Ti_{0.96}, Mo_{0.04})C_{0.67}$ exhibits

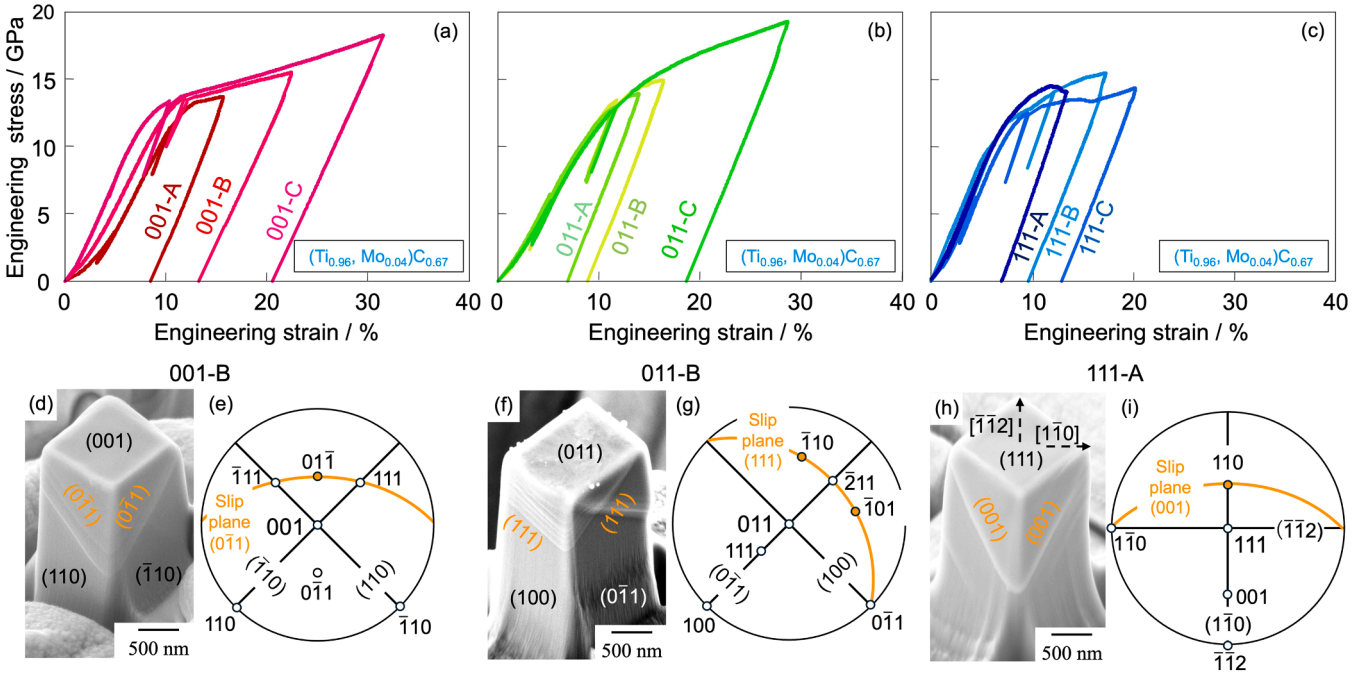

Fig. 4. (a–c) Stress–strain curves of the $(Ti_{0.96}, Mo_{0.04})C_{0.67}$ specimen obtained from the micropillar compression test along the <001>, <011>, and <111> compression directions. (d, f, h) SEIs of the specimens after the test, and (e, g, i) Corresponding stereographic analyses of the slip lines. The pillar names are shown along the stress–strain curves.

Table 1
Compression directions, slip systems, yield stresses, and CRSS data obtained from the micropillar compression tests of the $(Ti_{0.96}, Mo_{0.04})C_{0.67}$ specimen.

Pillar name	Compression direction	Slip system	Yield stress (GPa)	CRSS (GPa)
001-A	<1 7 29>	{110}<1$\bar{1}$0>	11.6	5.5
001-B	<1 1 33>		11.8	5.9
001-C	<1 1 12>		11.3	5.5
011-A	<0 11 12>	{111}<1$\bar{1}$0>	10.2	4.3
011-B	<0 10 11>		11.2	4.8
011-C	<1 19 20>		10.1	4.2
111-A	<13 15 116>	{001}<1$\bar{1}$0>	10.6	5.2
111-B	<10 10 11>		9.7	4.7

superior deformability owing to its off-stoichiometry. The CRSS of each slip system decreased in the following order: {110}<1$\bar{1}$0> (5.6 GPa), {001}<1$\bar{1}$0> (5.0 GPa), and {111}<1$\bar{1}$0> (4.4 GPa).

In TiC, only the {110}<1$\bar{1}$0> slip system is active at room temperature, resulting in brittle behavior. However, at high temperatures, the {111}<1$\bar{1}$0> slip system also becomes active, leading to ductile behavior [21,22]. For the $(Ti_{0.96}, Mo_{0.04})C_{0.67}$ specimen, {001}<1$\bar{1}$0>, {110}<1$\bar{1}$0>, and {111}<1$\bar{1}$0> slip systems were identified at room temperature, and the material exhibited ductile behavior.

The activation of these slip systems was further validated using the Schmid factor. Table 2 shows the Schmid factors calculated from the observed compression direction and the slip system, as well as from the normal stress calculated using the CRSS for each slip system measured in the micropillar test. The normal stress for the dislocations to glide in the slip system was estimated by dividing the average experimental CRSS value (Table 1) by the Schmid factor. The slip system with the lowest normal stress should be active. The slip systems with the lowest normal stresses in the <011> and <111> compression directions were {111}<1$\bar{1}$0> and {001}<1$\bar{1}$0> slip systems, respectively, consistent with the experimental results. In the [001] direction, the calculated normal stresses of the {110} and {111} slip systems were almost identical, although the latter system exhibited slightly lower values. This observation contrasts with the experimental results. Two possible reasons for this discrepancy are experimental error and the assumption that the CRSS of each slip system is independent of the orientation. However, in terms of the Schmid factor, the activation of slip systems observed in the micropillar compression test was reasonable.

Fig. 5 shows the SEIs of the test specimens after the micropillar compression tests. In the <001> compression direction, no cracks were observed, even when 20 % plastic strain was introduced (Figs. 5(a) and 5 (b)). In the <011> compression direction, no cracks were observed, even when ~10 % plastic strain was introduced in the 011-B direction (Fig. 5(c)). However, in the case of the 011-C compression direction,

Table 2
Schmid factors for the slip systems of $(Ti_{0.96}, Mo_{0.04})C_{0.67}$, and the corresponding stresses required to initiate plastic deformation. The slip systems indicated by bold numbers were active in the micropillar compression tests.

Compression direction	Slip system					
	{001}<1$\bar{1}$0>		{110}<1$\bar{1}$0>		{111}<1$\bar{1}$0>	
	Schmid factor	Calculated normal stress (GPa)	Schmid factor	Calculated normal stress (GPa)	Schmid factor	Calculated normal stress (GPa)
001	0	∞	**0.5**	**11.2**	0.41	10.7
011	0.35	14.3	0.25	22.4	**0.41**	**10.7**
111	**0.47**	**10.6**	0	∞	0.27	16.3

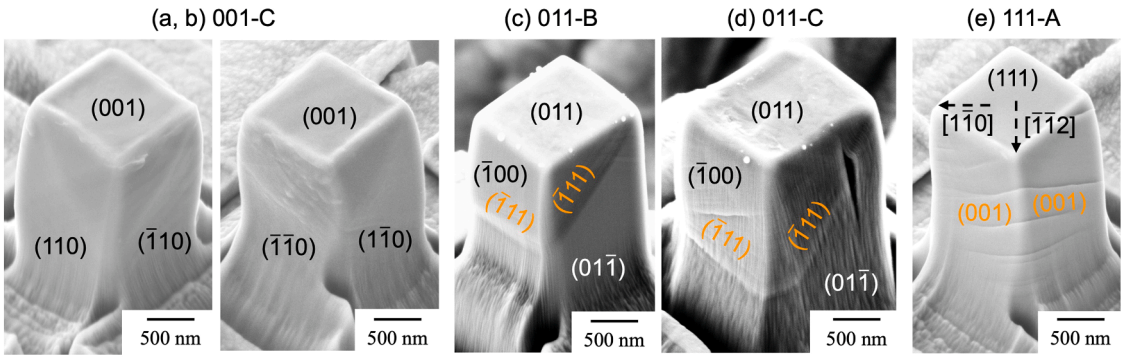

Fig. 5. SEIs of the $(Ti_{0.96}, Mo_{0.04})C_{0.67}$ specimen after the micropillar compression tests along the (a, b) 001-C, (c) 011-B, (d) 011-C, and (e) 111-A compression directions. The images shown in panels (c) and (e) correspond to the rear sides of the samples in Figs. 4(f) and 4(h), respectively.

where a plastic strain of up to ~20 % was introduced, crack initiation was observed parallel to the {001} plane (Fig. 6(d)). Furthermore, cracks were observed on the {001} plane in the <111> compression direction at a lower strain level than those in the <001> and <011> compression directions (Figs. 5(e)). Consequently, as in the case of the stoichiometric TiC, the cleavage fracture plane of $(Ti_{0.96}, Mo_{0.04})C_{0.67}$ was also identified as the {001} plane [13,14]. Notably, in the <111> compression direction, because the {001} plane is both a cleavage plane and a slip plane, cracks can form upon the application of lower strains compared to those required in the other compression directions.

3.3. *Effect of off-stoichiometry on deformation in TiC in Mo-Ti-C ternary system*

In contrast to stoichiometric TiC, which exhibited complete fracture at a relatively early stage of deformation, $(Ti_{0.96}, Mo_{0.04})C_{0.67}$ deformed under >10 % plastic strain without fracture. This indicates that the plastic deformability of $(Ti_{0.96}, Mo_{0.04})C_{0.67}$ was enhanced because of off-stoichiometry. The yield stress of $(Ti_{0.96}, Mo_{0.04})C_{0.67}$ was significantly lower than that of the stoichiometric TiC. The reduction in yield stress could contribute to the improvement of plastic deformability and the suppression effect of crack propagation. In addition, the {001}<$1\bar{1}0$>, {011}<$1\bar{1}0$>, and {111}<$1\bar{1}0$> slip systems were activated during the plastic deformation of $(Ti_{0.96}, Mo_{0.04})C_{0.67}$, and the CRSS values of these slip systems decreased in the following order: {110}<$1\bar{1}0$> (5.6 GPa), {001}<$1\bar{1}0$> (5.0 GPa), and {111}<$1\bar{1}0$> (4.4 GPa).

The ease of dislocation gliding was correlated with the Peierls stress, which is defined as the shear stress required to glide a dislocation. More specifically, the Peierls stress (τ_p) was calculated using the following equation [47–49]:

$$\tau_p = \frac{2G}{(1-\nu)} \exp\left[-\frac{\pi h}{(1-\nu)b}\right] \quad (1)$$

where G is the shear modulus, ν is the Poisson's ratio, h is the spacing of the glide plane, and b is the magnitude of the Burgers vector. Table 3 summarizes the calculated τ_p for each slip system of TiC and $(Ti_{0.96}, Mo_{0.04})C_{0.67}$. Notably, the results obtained for the [001] compression direction in TiC were not included in the analysis because a large number of cracks were present. The Poisson's ratio was assumed to be orientation-independent, and the results from a previous study were used as reference [43]. The shear modulus for each direction was calculated from the average Young's modulus (obtained from the micropillar compression test) and the Poisson's ratio, assuming an isotropic elastic body. The calculated τ_p value of $(Ti_{0.96}, Mo_{0.04})C_{0.67}$ was significantly lower than that of TiC, consistent with the experimental results, indicating a notable decrease in the yield stress due to the off-stoichiometry of $(Ti_{0.96}, Mo_{0.04})C_{0.67}$. Therefore, the decrease in shear modulus is the primary factor contributing to the reduction in yield stress, the improvement in plastic deformability, and the suppression of crack propagation.

However, the τ_p of $(Ti_{0.96}, Mo_{0.04})C_{0.67}$ on the {111}<$1\bar{1}0$> slip system was higher than those of the other slip systems, which is inconsistent with the experimental results, wherein the lowest CRSS was observed for the {111}<$1\bar{1}0$> slip system. Although the (111) plane of B1-type TiC is composed of alternating layers of Ti and C, vacancy-rich TiC forms a vacancy-ordered structure, such as the R$\bar{3}$m-type ordered structure, in which the C layer of the (111) plane in the B1-type structure is replaced with alternating C and vacancy layers [50–52]. Previously, Tsurekawa et al. reported that $TiC_{0.59}$ forms an R$\bar{3}$m-type ordered structure [52], wherein the atomic plane spacing on the (111) plane of Ti, sandwiched between layers composed of vacancies only, was twice that of the B1-type structure. These results suggest that the dislocations in $(Ti_{0.96}, Mo_{0.04})C_{0.67}$ glide along the {111} slip plane of the R$\bar{3}$m-type ordered structure, resulting in the lowest τ_p value. Although this calculation involves several assumptions, the calculated slip system

Table 3
Calculated Peierls stresses for the TiC and $(Ti_{0.96}, Mo_{0.04})C_{0.67}$ specimens along each slip system. The values of the elements used in the calculation are also summarized.

Slip system	Young's modulus in the normal direction of the slip plane (GPa)	Shear modulus in the normal direction of the slip plane (GPa)	Poisson's ratio	Interplanar distance of the slip plane	Peierls stress (GPa)
{110}<$1\bar{1}0$> in TiC	342	141	0.21	$\sqrt{2}/4a$	48.8
{111}<$1\bar{1}0$> in TiC	320	132	0.21	$\sqrt{3}/6a$	65.8
{001}<$1\bar{1}0$> in $(Ti_{0.96}, Mo_{0.04})C_{0.67}$	194	77	0.26	1/2a	10.3
{110}<$1\bar{1}0$> in $(Ti_{0.96}, Mo_{0.04})C_{0.67}$	201	80	0.26	$\sqrt{2}/4a$	25.8
{111}<$1\bar{1}0$> in $(Ti_{0.96}, Mo_{0.04})C_{0.67}$	216	86	0.26	$\sqrt{3}/6a$	40.9
{111}<$1\bar{1}0$> in $(Ti_{0.96}, Mo_{0.04})C_{0.67}$ with ordered structure	216	86	0.26	$\sqrt{3}/3a$	7.2

dependence of τ_p is consistent with the experimentally measured slip system dependence of CRSS. These results demonstrate that the dislocations in $(Ti_{0.96}, Mo_{0.04})C_{0.67}$ were also able to activate the {111}<$1\bar{1}0$> and {001}<$1\bar{1}0$> slip systems (in addition to the {110}<$1\bar{1}0$> slip system) as a result of the significant decrease in τ_p caused by the reduced elastic modulus and the vacancy-ordered structure. Observation of the lowest CRSS for the {111}<$1\bar{1}0$> slip system may therefore be attributed to the vacancy-ordered structure.

4. Conclusions

In this study, the deformation and fracture behaviors were investigated for $(Ti_{0.96}, Mo_{0.04})C_{0.67}$, which exists in equilibrium with a Mo solid solution and stoichiometric TiC. To investigate the deformation behavior, micropillar compression tests utilizing an in situ scanning electron microscope were performed. It was found that the yield stress of $(Ti_{0.96}, Mo_{0.04})C_{0.67}$ was significantly lower than that of the stoichiometric TiC. In addition, the {001}<$1\bar{1}0$>, {011}<$1\bar{1}0$>, and {111}<$1\bar{1}0$> slip systems were identified to be active during the plastic deformation of $(Ti_{0.96}, Mo_{0.04})C_{0.67}$, and the critical resolved shear stress values of these slip systems decreased in the following order: {110}<$1\bar{1}0$> (5.6 GPa), {001}<$1\bar{1}0$> (5.0 GPa), and {111}<$1\bar{1}0$> (4.4 GPa). In contrast to the stoichiometric TiC, which exhibited complete fracture at a relatively early stage of deformation, $(Ti_{0.96}, Mo_{0.04})C_{0.67}$ deformed under >10 % plastic strain without fracturing, with cracks preferentially initiating along the {001} plane. These results indicate that the off-stoichiometry of $(Ti_{0.96}, Mo_{0.04})C_{0.67}$ improves plastic deformability and has a suppressive effect on crack propagation. The enhanced deformability may be attributed to the significantly reduced shear modulus caused by off-stoichiometry.

CRediT authorship contribution statement

Shuntaro Ida: Data curation, Funding acquisition, Investigation, Validation, Writing – original draft, Writing – review & editing. **Eri Nakagawa:** Investigation. **Viola Paul:** Investigation. **Takahito Ohmura:** Investigation, Resources, Writing – original draft, Writing – review & editing. **Kyosuke Yoshimi:** Funding acquisition, Project administration, Resources, Writing – original draft, Writing – review & editing.

Declaration of competing interest

The authors declare that they have no known competing financial interests or personal relationships that could have appeared to influence the work reported in this paper.

Acknowledgements

This work was supported by the NIMS Joint Research Hub Program and the Light Metal Education Foundation, JSPS KAKENHI [grant number JP24K17526]; and the MEXT Program: Data Creation and Utilization-Type Material Research and Development Project [grant number JPMXP1122684766].

References

[1] E.K. Storms, The Refractory Carbides, Academic Press, New York, 1967.
[2] A. Rajabi, M.J. Ghazali, A.R. Daud, Chemical composition, microstructure and sintering temperature modifications on mechanical properties of TiC-based cermet A review, Mater. Des. 67 (2015) 95–106, https://doi.org/10.1016/j.matdes.2014.10.081.
[3] R. Subramanian, J.H. Schneibel, Processing iron-aluminide composites containing carbides or borides, JOM 49 (1997) 50–53.
[4] N.A. Dubrovinskaia, L.S. Dubrovinsky, S.K. Saxena, R. Ahuja, B. Johansson, High-pressure study of titanium carbide, J. Alloys Compd. 289 (1999) 24–27.
[5] J. Garcia, R. Pitonak, The role of cemented carbide functionally graded outer-layers on the wear performance of coated cutting tools, Int. J. Refract. Met. Hard Mater. 36 (2013) 52–59.
[6] S. Veprek, M.G.J. Veprek-Heijman, P. Karvankova, J. Prochazka, Different approaches to superhard coatings and nanocomposites, Thin Solid Films 476 (2005) 1–29.
[7] N. Durlu, Titanium carbide-based composites for high temperature applications, J. Eur. Ceram. Soc. 19 (1999) 2415–2419.
[8] M. LeFlem, A. Allemand, S. Urvoy, D. Cédat, C. Rey, Microstructure and thermal conductivity of Mo–TiC cermets processed by hot isostatic pressing, J. Nucl. Mater. 380 (2008) 85–92.
[9] B.G. Compton, F.W. Zok, Impact resistance of TiC-based cermets, Int. J. Impact Eng. 62 (2013) 75–87.
[10] H. Endo, M. Ueki, H. Kubo, Microstructure and mechanical properties of hot-pressed SiC-TiC composites, J. Mater. Sci. 26 (1991) 3769–3774.
[11] C. Maerky, M.-O. Guillou, J.L. Henshall, R.M. Hooper, Indentation hardness and fracture toughness in single crystal $TiC_{0.96}$, Mater. Sci. Eng. A 209 (1996) 329–336.
[12] S. Ida, K. Watanabe, K. Yoshimi, Solidification microstructure and mechanical properties of B1-type TiC in Fe-Ti-C ternary alloys, ISIJ Int 64 (11) (2024) 1723–1731.
[13] by J.J. Gilman, Fracture, in: B.L. Averbach, D.K. Felbeck, G.T. Hahn, D.A. Thomas (Eds.), M.I.T. Technology Press, Cambridge, 1959, p. 193.
[14] by J.J. Gilman, Physical nature of plastic flow and fracture, in: E.H. Lee, P. S. Symonds (Eds.), Pergamon Press, Oxford, 1960, p. 43.
[15] A. Arya, E.A. Carter, Structure, bonding, and adhesion at the TiC(100)/Fe(110) interface from first principles, J. Chem. Phys. 118 (19) (2003) 8982–8996, https://doi.org/10.1063/1.1565323.
[16] J. Dong, D. Hou, J. Li, R. Huang, Investigation of NbC/TiC heterogeneous nucleation interface by first-principles and experimental methods, Metals (Basel) 9 (2019) 1265, https://doi.org/10.3390/met9121265.
[17] D.J. Rowcliffe, G.E. Hollox, Hardness anisotropy, deformation mechanisms and brittle to ductile transition in carbides, J. Mater. Sci. 6 (1971) 1270–1276.
[18] N. De Leon, X.-X. Yu, H. Yu, C.R. Weinberger, G.B. Thompson, Bonding effect on the slip differences in the B1 monocarbides, Phys. Rev. Lett. 114 (2015) 165502.
[19] C.J. Smith, X.-X. Yu, Q. Guo, C.R. Weinberger, G.B. Thompson, Phase, hardness, and deformation slip behavior in mixed HfxTa1-xC, Acta Mater 145 (2018) 142–153.
[20] G. Morgan, M.H. Lewis, Hardness anisotropy in niobium carbide, J. Mater. Sci. 9 (1974) 349–358.
[21] D.K. Chatterjee, M.G. Mendiratta, H.A. Lipsitt, Deformation behaviour of single crystals of titanium carbide, J. Mater. Sci. 14 (1979) 2151–2156.
[22] S. Tsurekawa, H. Yoshinaga, Dislocation dissociation in titanium carbide crystal, J. Jpn. Inst. Metals 58 (1994) 390–396.
[23] T. Csanádi, E. Castle, M.J. Reece, J. Dusza, Strength enhancement and slip behaviour of high-entropy carbide grains during micro-compression, Sci. Rep. 9 (2019) 10200.
[24] J.-E. Sundgren, Structure and properties of TiN coatings, Thin Solid Films 128 (1985) 21–44.
[25] W.S. Williams, Scattering of electron by vacancy in nonstoichiometric crystals of titanium carbide, Phys. Rev. A 135 (1964) A505–A510.
[26] W.S. Williams, Transition-metal carbides, Prog. Solid State Chem. 6 (1971) 57–118.
[27] W.S. Williams, Transition metal carbides, nitrides, and borides for electronic applications, JOM 49 (1997) 38–42.
[28] H.W. Hugosson, P. Korzhavyi, U. Jansson, B. Johansson, O. Eriksson, Phase stabilities and structural relaxations in stoichiometric TiC_{1-x}, Phys. Rev. B 63 (2001) 1651116.
[29] P.A. Korzhavyi, L.V. Pourovskii, H.W. Hugosson, A.V. Ruban, B. Johansson, Ab initio study of phase equilibria in TiC_x, Phys. Rev. Lett. 88 (2002) 015505.
[30] Z. Dridi, B. Bouhaf, P. Ruterana, H. Aourag, First-principles calculations of vacancy effects on structural and electronic properties of TiC_x and TiN_x, J. Phys. Condens. Matter 14 (2002) 10237–10249.
[31] X.-X. Yu, G.B. Thompson, C.R. Weinberger, Influence of carbon vacancy formation on the elastic constants and hardening mechanisms in transition metal carbides, J. Eur. Ceram. Soc. 35 (2015) 95–103.
[32] R.G. Lye, E.M. Logothetis, Optical properties and band structure of titanium carbide, Phys. Rev. 147 (1966) 622–635.
[33] L. Ramqvist, K. Hamrin, G. Johansson, U. Gelius, C. Nordling, VC, NbC and TaC with varying carbon content studied by ESCA, J. Phys. Chem. Solids 31 (1970) 2669–2672.
[34] H. Kindlund, D.G. Sangiovanni, J. Lu, J. Jensen, V. Chirita, J. Birch, I. Petrov, J. E. Greene, L. Hultman, Vacancy-induced toughening in hard single-crystal $V_{0.5}Mo_{0.5}N_x$/MgO(001) thin films, Acta Mater 77 (2014) 394–400.
[35] V.I. Razumovskiy, A.V. Ruban, J. Odqvist, D. Dilner, P.A. Korzhavyi, Effect of carbon vacancies on thermodynamic properties of TiC–ZrC mixed carbides, CALPHAD: Comput. Coupling Phase Diagrams Thermochem. 46 (2014) 87–91.
[36] B. Jiang, K. Huang, J. Hou, S. Jiao, H. Zhu, Experimental and first-principles study of Ti-C-O system: interplay of thermodynamic and structural properties, J. Am. Ceram. Soc. 100 (2017) 2253–2265.
[37] S.-H. Jhi, J. Ihm, S.G. Louie, M.L. Cohen, Electronic mechanism of hardness enhancement in transition-metal carbonitrides, Nature 399 (1999) 132–134.
[38] D. Edström, D.G. Sangiovanni, L. Hultman, I. Petrov, J.E. Greene, V. Chirita, Elastic properties and plastic deformation of TiC- and VC-based pseudobinary alloys, Acta Mater 144 (2018) 376–385.
[39] Y. Li, H. Katsui, T. Goto, Phase decomposition of (Ti, Zr)(C, N) solid solutions prepared by spark plasma sintering, J. Eur. Ceram. Soc. 39 (2019) 4588–4594.

[40] Z. Cap, N. Jin, J. Ye, X. Du, Y. Liu, First-principles study on the effects of N and Al doping on the mechanical properties and electronic structures of TiC, 10, RSC Adv, 2020 36295.
[41] V.I. Ivashchenko, A.A. Onoprienko, P.L. Scrynskyy, A.O. Kozak, V.I. Shevchenko, M. Tapajna, L. Orovčík, P.M. Lytvyn, N.R. Medykh, Structural, mechanical, optoelectronic and thermodynamic properties of bulk and film materials in Ti–Nb–C system: first principles and experimental investigations, Phys. B 646 (2022) 414311.
[42] S. Ida, N. Sekido, K. Yoshimi, Solidification pathways and phase equilibria in the Ti-Mo-C ternary system, High Temp. Mater. Processes 39 (2020) 164–170.
[43] S. Ida, K. Hoshizaki, T. Kaneko, X. Nan, N. Sekido, K. Yoshimi, Off-stoichiometry and molybdenum substitution effects on elastic moduli of B1-type titanium carbide, Sci. Rep. 13 (2023) 13631.
[44] D.G. Pettifor, Theoretical predictions of structure and related properties of intermetallics, Mater. Sci. Technol. 8 (1992) 345–349.
[45] F. Pugh, XCII Pugh, Relations between the elastic moduli and the plastic properties of polycrystalline pure metals, London Edinburgh Philos, Mag. & J. Sci 45 (367) (1954) 823–843.
[46] C. Kral, W. Lengauer, D. Rafaja, P. Ettmayer, Critical review on the elastic properties of transition metal carbides, nitrides and carbonitrides, J. Alloys Compd. 265 (1998) 215–233.
[47] R.E. Peierls, The size of a dislocation, Proc. Phys. Soc. 52 (1940) 34–37.
[48] F.R.N. Nabarro, Dislocations in a simple cubic lattice, Proc. Phys. Soc., London 59 (1947) 256–272.
[49] H.B. Huntington, Modification of the Peierls-Nabarro model for edge dislocation core, Proc. Phys. Soc. B68 (1955) 1043.
[50] V. Moisy-Maurice, N. Lorenzelli, C.H. De Novion, P. Convert, High temperature neutron diffraction study of the order-disorder transition in TiC_{1-x}, Acta Metall 30 (9) (1982) 1769–1779.
[51] R. Eibler, New aspects of the energetics of ordered Ti_2C and Ti_2N, J. Phys. Condens. Matter 19 (2007) 196226.
[52] S. Tsurekawa, H. Yoshinaga, Identification of long range ordered structure in $TiC_{0.59}$ by transmission electron microscopy, J. Jpn. Inst. Metals 56 (1992) 133–141.